This article has been accepted for publication in a future issue of this journal, but has not been fully edited. Content may change prior to final publication. Citation information: DOI 10.1109/JSTARS.2020.3022726, IEEE Journal of Selected Topics in Applied Earth Observations and Remote Sensing

A New Metric for Estimating the Disparity of Antenna Patterns in Synthetic Aperture Imaging Radiometry

Éric Anterrieu, Baptiste Palacin and Laurent Costes

***Abstract*— The Soil Moisture and Ocean Salinity (SMOS) satellite has provided for about 10 years systematic passive L-band measurements from space. For several months, phase 0 studies are conducted by the French space agency for a second generation High Resolution (HR) follow-on mission. This contribution is making the connection between this SMOS*hr* project and the SMOS mission by revisiting the following problematic: the impact of the disparity of the antenna patterns on the reconstruction floor error observed in the retrieved brightness temperatures. This impact is revisited in light of the progress made since that time and a new metric is introduced for estimating the disparity between antenna patterns. It would be helpful for the design of future missions based on imaging by aperture synthesis with interferometric arrays comprising a large number of antennas.**

***Index Terms*— Imaging radiometry, aperture synthesis, interferometric array, antenna pattern.**

I. Introduction

The Soil Moisture and Ocean Salinity (SMOS) space mission [1] was launched in November 2009 by ESA and CNES and for almost a decade this 1st generation satellite has provided accurate radiometric brightness temperature maps with a spatial resolution of $\sim$50 km at L-band. These maps have been used for retrieving surface soil moisture (SM) [2] as well as ocean salinity (OS) [3]. In addition, these brightness temperatures are operationally monitored at the European Centre for Medium-Range Weather Forecasts (ECMWF) [4].

For about two years, phase 0 studies are conducted by the French space agency for a 2nd generation High Resolution (HR) follow-on mission [5]. The goal of this SMOS*hr* project is to ensure the continuity of L-band measurements while increasing the spatial resolution to $\sim$10 km, without degrading the radiometric sensitivity and keeping the revisit time of 3 days unchanged. This would require a typical antenna size of $\sim$18 m. Taking into account the difficulty of deployment of a real aperture of this size in space [6] and the successful alternative approach used for SMOS [7], the 2nd generation SMOS*hr* will also perform aperture synthesis [8] with three times more antennas than SMOS has [9].

This work is making the connection between the two generations, the present SMOS and the future SMOS*hr*, by revisiting a problematic that was discovered too late in the SMOS project for being solved in due time. This issue concerns the impact of the disparity of the antenna patterns [10] on the reconstruction floor error observed in the retrieved brightness temperatures [11]. The observing equation of an imaging radiometer by aperture synthesis is recalled in section II. The impact of the disparity of the antenna patterns is revisited in section III in light of the progress made since the time this issue was observed with SMOS. A new metric is introduced in section IV for estimating the disparity between antenna patterns. It is illustrated with the antenna patterns of SMOS measured prior launch in an anechoic chamber [12]. Finally, it is shown how this new metric would have been useful for detecting those antennas in the interferometric array with a pattern outside a confidence region and which contribute too much to the reconstruction floor error and therefore to the degradation of the mission performances.

Manuscript submitted May 15th, 2020; revised Aug. 15th, 2020; accepted Aug. 26th, 2020.

This work is supported by Research and Technology initiatives from the Centre National d'Études Spatiales (CNES) for the Centre d'Études Spatiales de la BIOsphère (CESBIO) and for Airbus Defence and Space (ADS) within the frame of the SMOS*hr* project.

E. Anterrieu is with Centre d'Études Spatiales de la BIOsphère (CESBIO), 13 avenue Colonel Roche, 31400 Toulouse, France.

B. Palacin is with Centre National d'Études Spatiales (CNES), 18 avenue Edouard Belin, 31400 Toulouse, France.

L. Costes is with Airbus Defence and Space (ADS), 31 rue des Cosmonautes, 31400 Toulouse, France.

e-mail: Eric.Anterrieu@cesbio.cnes.fr

Digital Object Identifier 10.1109/????.2020.??????

II. Observing equation of interferometric arrays

While classical radiometers measure the power collected by a highly directive antenna, interferometric measurements with an aperture synthesis radiometer are obtained by cross-correlating the signals collected by pairs of non-directive antennas having overlapping fields of view. As a consequence, if total power radiometers provide direct measurements of the brightness temperature in the main beam direction of the antenna, aperture synthesis ones required inversion of the so-called complex visibilities [13] with the aid of the computer in order to retrieve the brightness temperature distribution in front of the instrument [14]. The collection of antennas, also referred as the interferometric array in aperture synthesis, as well as their characteristics, play a key role in this inversion process and therefore in the performances of the instrument.

The relationship between the complex visibilities and the brightness temperature of the scene under observation has been revisited in order to take into account the mutual coupling of close antennas [13]. Without polarimetric considerations [15], the complex visibility V_{pq} for a pair of antennas $\mathcal{A}_p$ and $\mathcal{A}_q$

This article has been accepted for publication in a future issue of this journal, but has not been fully edited. Content may change prior to final publication. Citation information: DOI 10.1109/JSTARS.2020.3022726, IEEE Journal of Selected Topics in Applied Earth Observations and Remote Sensing

is given by:

$$V_{pq} = \frac{1}{\sqrt{\Omega_p \Omega_q}} \iint_{\xi^2+\eta^2 \leq 1} F_p(\xi,\eta)\overline{F}_q(\xi,\eta)\big(T_b(\xi,\eta) - T_{rec}\big) \times \widetilde{r}_{pq}(t) \frac{\mathrm{e}^{-2\mathrm{j}\pi(u_{pq}\xi + v_{pq}\eta + w_{pq}\sqrt{1-\xi^2-\eta^2})}}{\sqrt{1-\xi^2-\eta^2}} \mathrm{d}\xi\mathrm{d}\eta, \quad (1)$$

where (u_{pq}, v_{pq}, w_{pq}) are the components of the baseline vector $\mathbf{b}_{pq}$ normalized to the central wavelength of observation λ, $\xi = \sin\theta\cos\phi$ and $\eta = \sin\theta\sin\phi$ are direction cosines in the reference frame of the arrays, θ and ϕ are the classical spherical co-ordinates (the colatitude and the azimuth, respectively), T_{rec} is the physical temperature of the receivers (assumed to be the same for all the receivers), F_p and F_q are the normalized voltage patterns of the two antennas with equivalent solid angles Ω_p and Ω_q (the overbar indicates the complex conjugate), $\widetilde{r}_{pq}$ is the fringe-washing function which accounts for spatial decorrelation effects and finally $t = (u_{pq}\xi + v_{pq}\eta + w_{pq}\sqrt{1-\xi^2-\eta^2})/f$ is the spatial delay with $f = c/\lambda$ the central frequency of observation.

Referring back to (1), after discretization of the integral over an appropriate sampling grid in the direction cosines domain, the relationship between the complex visibilities V and the brightness temperature distribution T_b of the scene under observation can be written in the linear form:

$$V = \mathbf{G}T, \quad (2)$$

where $\mathbf{G}$ is the modeling operator of the instrument. The inverse problem aims at retrieving $T = T_b$ (the constant T_{rec} is cancel out from the visibilities with the aid of the response to a flat target [16], whatever the method used for the inversion [17]). As this inverse problem is ill-posed, it has to be regularized in order to provide a unique and stable solution for T. Among the regularization methods, the minimum-norm solution is widely used in imaging radiometry [18]:

$$T_r = \min_T \|T\|^2 \text{ s.t. } \mathbf{G}T = V. \quad (3)$$

This map is obtained through the computation of the pseudo-inverse $\mathbf{G}^+$ of $\mathbf{G}$:

$$T_r = \mathbf{G}^+ V, \quad (4)$$

where $\mathbf{G}^+$ is computed with the aid of a truncated singular values decomposition of $\mathbf{G}$ which discards the smallest singular values prior the inversion. In order to filter out the Gibbs effects due to the sharp frequency cut-off associated to the limited extent of the experimental frequency coverage H of the instrument, T_r has to be damped by an appropriate windowing function: $\mathcal{T}_r = W \star T_r$ [19]. This map has to be compared to $\mathcal{T}_w = W \star T_b$ (which is the "ideal" temperature map to be reconstructed and apodized with the same window W) and not to T_b (which is not at the same spatial resolution).

Early in the project of the SMOS mission, numerical simulations have been conducted to analyze the performances of the inversion process. A systematic error has been observed in the retrieved brightness temperature maps when comparing $\mathcal{T}_r$ to $\mathcal{T}_w$, although no modeling errors were introduced in $\mathbf{G}$ and no noise was added to V. It has been shown that this reconstruction floor error cannot be attributed to the high frequencies components of the scene T_b since they are filtered out by the instrument itself. Two origins have been investigated [20]: an instrument dependent component which has revealed the key role played by the voltage patterns of the antennas [21], and a scene dependent component which has shown the influence of the aliased regions of the synthesized field of view [22]. If various approaches have been successfully proposed and implemented for reducing the effect of the latter component [23], nothing has been done for the former one [24].

III. Influence of Antenna Patterns

The influence of the antennas and especially that of the disparity of the voltage patterns F_p and F_q from one baseline $\mathbf{b}_{pq}$ to the other has been analyzed in [20] with the aid of numerical simulations conducted within the frame of the SMOS project. However, the antenna voltage patterns introduced in the modeling matrix $\mathbf{G}$ were derived from a very simple model [25] and were not the radiation patterns of the 69 antennas of SMOS which were not available at that time [12]. As there are evidences that models of radiation patterns do not reproduce measurements made on antennas in an anechoic chamber, this study is briefly revisited hereafter.

Shown on Figure 1 are the distributions of the singular values of the operator $\mathbf{G}$ with the current modeling of SMOS instrument which includes those antenna patterns measured prior launch [12]. As the average pattern $\langle F \rangle$ plays a key role in the analysis, the same distribution is shown for a virtual instrument like SMOS but equipped with equal antennas sharing the same voltage pattern $\langle F \rangle$. In both cases, there are clearly two groups of singular values with a very well-determined gap in between: this situation has been already explained [26]. Although here the two modeling operators are sharing exactly the same first group of singular values, the second groups with the smallest ones are very different. Owing to the role played by these smallest singular values in the pseudo-inversion of $\mathbf{G}$, only those lying in the first group

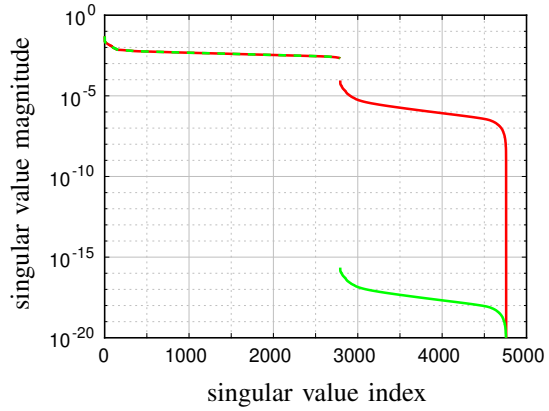

Fig. 1. Distributions of the singular values of the modeling operator $\mathbf{G}$ in X polarization. Two groups of singular values separated by a well-determined gap are observed. However, in the ideal case (green, same voltage pattern for each antenna), this gap is wider than in the present case of SMOS (red, 69 different antenna patterns). The same behavior is observed in Y polarization.

This article has been accepted for publication in a future issue of this journal, but has not been fully edited. Content may change prior to final publication. Citation information: DOI 10.1109/JSTARS.2020.3022726, IEEE Journal of Selected Topics in Applied Earth Observations and Remote Sensing

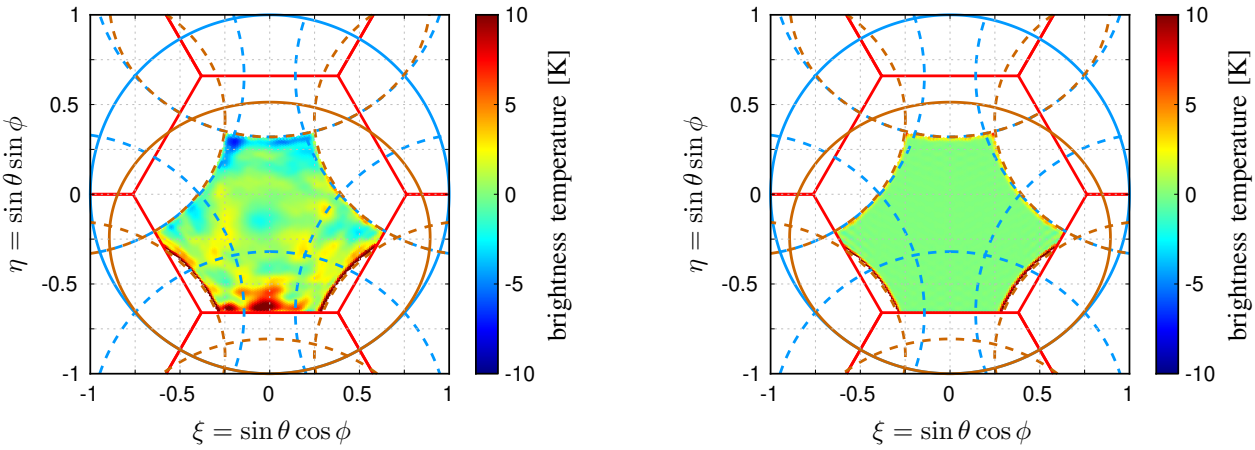

Fig. 2. Typical error maps $\mathcal{T}_r - \mathcal{T}_w$ of simulations performed in X polarization with the current modeling of SMOS (left, 69 different antenna patterns) and with that of a virtual instrument like SMOS (right, same voltage pattern for each antenna). With the disparity of the 69 antenna patterns of SMOS, the bias and the standard deviation of the error maps in that part of the field of view free from Earth aliases are respectively about 0.7 K and 1.8 K. On the contrary, when the disparity is reduced to zero they are respectively less than 0.01 K and 0.05 K. The same behavior is observed in Y polarization.

are kept in the computation of $\mathbf{G}^+$ with the aid of the so-called truncated singular value decomposition. As illustrated in Figure 2 with error maps $\mathcal{T}_r - \mathcal{T}_w$ corresponding to these two cases, the wider this gap between the two groups of singular values, the smaller is the reconstruction floor error. On this example, with the disparity of the 69 different antenna patterns F of SMOS, the bias and the standard deviation of the error maps are respectively about 0.7 K and 1.8 K whereas they are respectively less than 0.01 K and 0.05 K when the disparity is reduced to zero with equal antennas sharing the same voltage pattern $\langle F \rangle$.

Between these two extreme cases, intermediate situations can be studied by substituting $\langle F \rangle + (F - \langle F \rangle)/\alpha$ for each F as it is a convenient way to play with the disparity between the radiation patterns in the modeling of the instrument. The case of the present SMOS with 69 different antenna patterns is obtained with $\alpha = 1$. That of the previous instrument equipped with identical antennas sharing the same voltage pattern $\langle F \rangle$ is achieved when $\alpha \to +\infty$. For any $\alpha > 1$, the disparity between the 69 patterns is α times smaller than that of SMOS. On the contrary, for any $\alpha < 1$, it is $1/\alpha$ times larger. Thanks to this approach it is possible to study the impact of this disparity onto the inversion process. This is what is shown on Figure 3 where the bias and the standard deviation of reconstruction error maps $\mathcal{T}_r - \mathcal{T}_w$ are reported as a function of the parameter α. As suggested by the two cases reported in Figure 2, $\alpha = 1$ and $\alpha \to +\infty$, the reconstruction floor error is clearly a decreasing function of the parameter α: the larger the disparity between the 69 different patterns, the larger the bias and the standard deviation in the error maps.

The parameter α has been introduced for controlling the disparity between SMOS antenna patterns. Although it has been a useful approach for illustrating the impact of this disparity onto the reconstruction floor error, it is suffering from some drawbacks. The main negative point of this approach lies in its inability to quantify the disparity between the antenna patterns. It can only compare it to the one observed in the 69 antenna patterns of SMOS. Moreover, it cannot distinguish

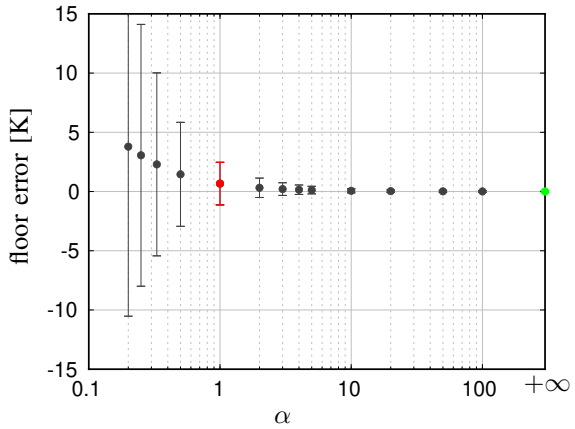

Fig. 3. Bias (bullets) and standard deviation (bars) of the floor error as a function of the factor α used for changing the disparity between the 69 radiation patterns in the modeling of an instrument like SMOS in X polarization. For $\alpha = 1$ the situation is that of SMOS (red) while for $\alpha \to +\infty$ it is that of an instrument like SMOS (green) but with the same voltage pattern for each antenna (these two cases are those illustrated in Figures 1 and 2). The reconstruction floor error is a decreasing function of α and when the disparity between the 69 radiation patterns is attenuated by a factor larger than 10 it becomes negligible. The same behavior is observed in Y polarization.

the patterns which are strong contributors to the reconstruction floor error from those contributing a little.

IV. Comparison of Antenna Patterns

There has been many attempts to define objective quantitative metrics of comparison between radiation patterns that can be used to assess the accuracy, the sensitivity and also the repeatability associated with the manufacturing of antennas [27]. None is perfect because they are all suffering from drawbacks. Many of these figures of merit are only suited for the comparison of power patterns because they are not sensitive to the phase pattern. Moreover, none of them has been specially designed for large data sets [28] like those involved in imaging radiometry by aperture synthesis (SMOS is equipped with 69 antennas [7], preliminary design studies of SMOS*hr*

This article has been accepted for publication in a future issue of this journal, but has not been fully edited. Content may change prior to final publication. Citation information: DOI 10.1109/JSTARS.2020.3022726, IEEE Journal of Selected Topics in Applied Earth Observations and Remote Sensing

are using 231 antennas [9]). There is a broad consensus that such a comparison is not an easy task. As a consequence, accounting for the remark drawn at the end of the last section, there is a need for such a metric for comparing large number of antennas and for having an objective way to reject those not satisfying specifications or quality requirements.

Parametric approaches have already been used in the attempt to self-characterize antenna patterns with few parameters [29]. However, they have never proven to be well adapted to experimental radiation patterns which are not rigorously reproduced by such models with too few parameters. As an example, when focusing on the main beam of the power patterns of the 69 antennas of SMOS, one cannot see any outliers in the distribution of the Half-Power Beam Width (HPBW) nor in that of the First Null Beam Width (FNBW). Nevertheless, a simple view at the 69 amplitude and phase patterns shows large discrepancies from one antenna to another. This example makes it clear that devil is in the details, details which are not seen nor reproduced by parametric approaches. As a consequence, this new metric should rely only on measurements and not on any radiation pattern modeling.

Coming back to the observing equation (1), the equivalent solid angle Ω of any antenna is given by:

$$\Omega = \iint_{\xi^2+\eta^2\leq 1} \frac{|F(\xi,\eta)|^2}{\sqrt{1-\xi^2-\eta^2}}\,\mathrm{d}\xi\mathrm{d}\eta. \quad (5)$$

As this definition involves the power pattern $|F|^2$ (see chap. 2 in [30]), Ω is a real-valued quantity although the voltage pattern F may be a complex-valued one. Keeping in mind the writing of (1), this definition suggests to introduce a similar quantity but for a pair of antennas $\mathcal{A}_p$ and $\mathcal{A}_q$ so that both antenna voltage patterns F_p and F_q contribute simultaneously to a unique complex value:

$$\Omega_{pq} \equiv \iint_{\xi^2+\eta^2\leq 1} \frac{F_p(\xi,\eta)\overline{F}_q(\xi,\eta)}{\sqrt{1-\xi^2-\eta^2}}\,\mathrm{d}\xi\mathrm{d}\eta, \quad (6)$$

which carries information on the amplitude and on the phase of the two voltage patterns. This new quantity can be named an "equivalent cross solid angle". It satisfies the conjugation relation $\Omega_{qp} = \overline{\Omega}_{pq}$ and it reduces to the standard equivalent solid angles $\Omega_p = \Omega_{pp}$ or $\Omega_q = \Omega_{qq}$ when $p = q$. As $\Omega_{pq}/\sqrt{\Omega_p\Omega_q}$ is a complex sesquilinear form, an inner product between two voltage patterns can be defined accordingly:

$$\langle F_p \mid F_q \rangle \equiv \frac{1}{\sqrt{\Omega_p\Omega_q}} \iint_{\xi^2+\eta^2\leq 1} \frac{F_p(\xi,\eta)\overline{F}_q(\xi,\eta)}{\sqrt{1-\xi^2-\eta^2}}\,\mathrm{d}\xi\mathrm{d}\eta. \quad (7)$$

When $F_p = F_q = F$ we therefore have $\langle F \mid F \rangle \equiv \|F\|^2 = 1$: the norm of any voltage pattern is equal to one according to this inner product. Although this remark is purely anecdotal because voltage patterns have nothing to do with them, this definition reminds that of the inner product between Chebyshev polynomials of the first kind [31]. Actually, this definition is very similar to that of the envelope correlation ρ_e defined by equation (1) in [32]. However, as $\rho_e \equiv |\langle F_p \mid F_q \rangle|^2$ is a real-valued quantity, the phase information transported by ρ_e is very limited compared to that carried by $\langle F_p \mid F_q \rangle$.

As the idea is not to compare all the antennas of an interferometric array to each other, but only to compare them to a given reference antenna $\mathcal{A}_{ref}$ in order to have a estimate of the distance between any voltage pattern F and the voltage pattern F_{ref} of the reference antenna, the following quantity is useful:

$$\langle F_{ref} \mid F \rangle \equiv \frac{1}{\sqrt{\Omega_{ref}\Omega}} \iint_{\xi^2+\eta^2\leq 1} \frac{F_{ref}(\xi,\eta)\overline{F}(\xi,\eta)}{\sqrt{1-\xi^2-\eta^2}}\,\mathrm{d}\xi\mathrm{d}\eta. \quad (8)$$

The reference antenna $\mathcal{A}_{ref}$ may be, for example, a specification given to a manufacturer or the output model of a simulation. In this contribution, the voltage pattern F_{ref} is the average voltage pattern $\langle F \rangle$ of the 69 radiation patterns F of SMOS that have been measured with accuracy [33] prior launch in an anechoic chamber [12]. The distribution of the corresponding inner products is therefore an indicator of the disparity of the 69 different patterns with respect to the average one: they are shown on Figure 4 in X and Y polarizations. If most patterns are confined inside the $3\,\sigma$ / 99.73% confidence ellipses, many of them are outside the $1\,\sigma$ / 68.27% ones [34]. The closer to $\|F_{ref}\|^2 \equiv 1$ is the complex value $\langle F_{ref} \mid F \rangle$, the closer this F is to F_{ref}. On the contrary, the farthest pattern from the reference pattern is that one whose $\langle F_{ref} \mid F \rangle$ is the farthest from 1. These patterns are shown in Figure 5 in X polarization: with a scalar product equal to $1.0013 + 0.0002i$, the closest one is that of antenna C20 (according to the naming of the antennas of SMOS found in Figure 1 of [35]). On the contrary, the farthest one is that of antenna AB03 with $0.9918 - 0.0886i$. The qualitative comparizon of the amplitude and phase patterns of these antennas is not in contradiction with what is deduced from this new metric. Similar results are obtained in Y polarization: the closest pattern is that of antenna B06 ($1.0012 + 0.0007i$) whereas the farthest one is that of antenna CA03 ($0.9918 - 0.0982i$).

Clearly identifiable on Figure 4 are the voltage patterns with their inner products outside the $1\,\sigma$ / 68.27% confidence

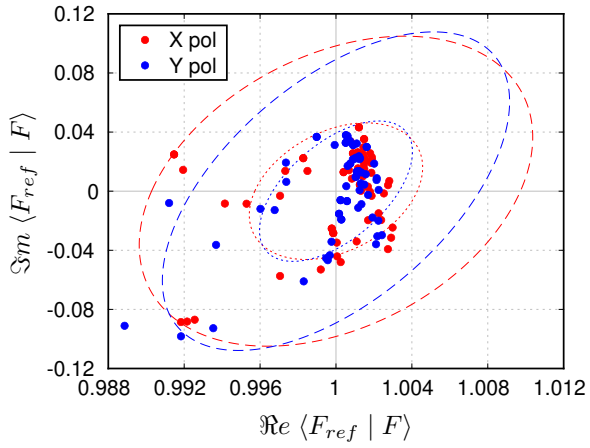

Fig. 4. Inner products (dots) between the voltage patterns F of the 69 antennas of SMOS and a reference voltage pattern F_{ref} (here equal to the average of the 69 radiation patterns) in X (red) and Y (blue) polarizations. The $1\,\sigma$ / 68.27% and the $3\,\sigma$ / 99.73% confidence ellipses of the complex-valued distributions $\langle F_{ref} \mid F \rangle$ are shown with dotted-lines and dashed-lines. The closer to $1 = \|F_{ref}\|^2$ is a dot, the closer the corresponding F is to F_{ref}. Attention should be paid on the different scales along both axis.

This article has been accepted for publication in a future issue of this journal, but has not been fully edited. Content may change prior to final publication. Citation information: DOI 10.1109/JSTARS.2020.3022726, IEEE Journal of Selected Topics in Applied Earth Observations and Remote Sensing

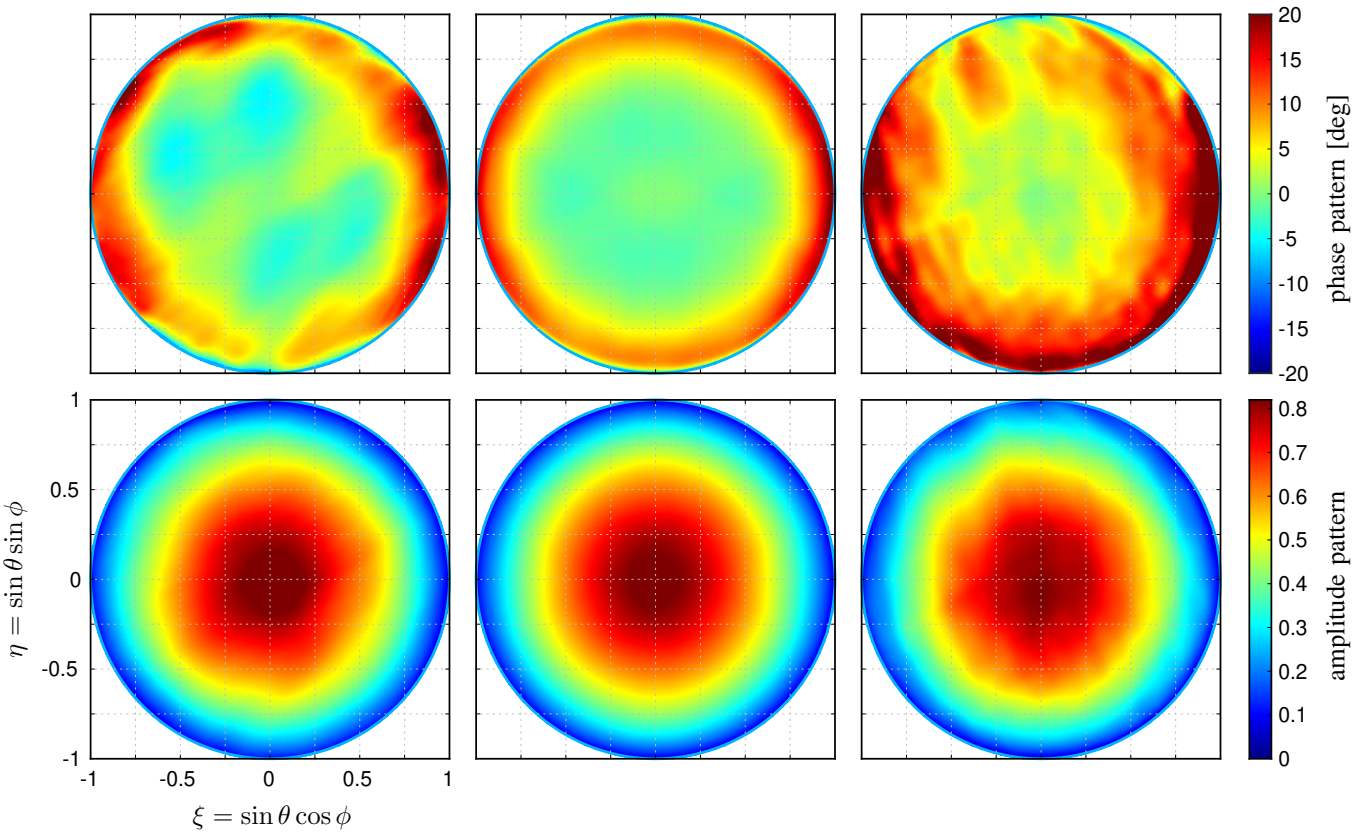

Fig. 5. Amplitude (bottom) and phase (top) patterns of three typical voltage patterns out of the 69 antennas of SMOS in X polarization: average pattern F_{ref} (center), patterns F closest to (left, antenna C20) and farthest from (right, antenna AB03) the average one according to the distance from the complex-valued scalar products $\langle F_{ref} \mid F\rangle$ to $\|F_{ref}\|^2 = 1$, as illustrated in Figure 4. Here $\langle F_{ref} \mid F_{\text{C20}}\rangle \simeq 1.0013 + 0.0002i$ and $\langle F_{ref} \mid F_{\text{AB03}}\rangle \simeq 0.9918 - 0.0886i$, so that these distances are respectively about 0.0013 for antenna C20 and 0.0890 for AB03 (whether by coincidence or not, that is a ratio close to 69).

ellipses: 15 in X polarization and 17 in Y polarization, out of 69, are concerned by this issue. The corresponding antennas are localized on SMOS instrument in Figure 6. Among the 22 unique antennas concerned, it should be noted that 10 are outside the confidence ellipse in both X and Y polarizations. If we were at the time of accepting or rejecting antennas coming out from an assembly chain, this new metric would suggest to pay attention to these ones and to take appropriate decisions. As this time is over, the present study can only be completed with simulations in order to check the impact of these patterns on the reconstruction floor error by reducing artificially their distance to the average pattern with the aid of the parameter α introduced in the previous section. Consequently, to be clear, as SMOS is now in orbit and visibilities have to be inverted with the same antenna patterns as those at the time they were measured, the modifications made hereafter are purely virtual, illustrative and in no way an improvement that could be brought to SMOS now.

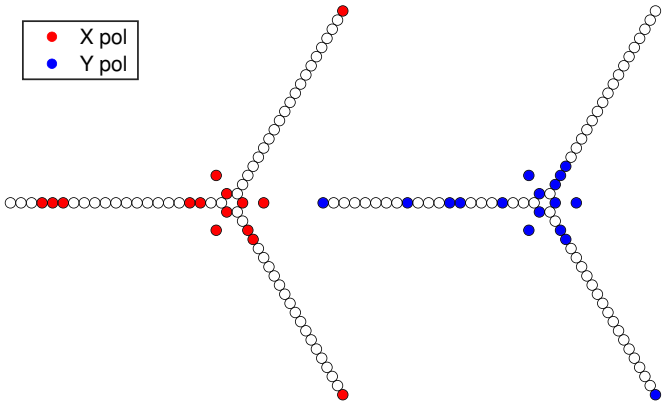

Fig. 6. Localization of the 15 antennas of SMOS in X polarization (red) and the 17 ones in Y polarization (blue) which have their voltage pattern F with an inner product $\langle F_{ref} \mid F\rangle$ outside the $1\,\sigma$ / 68.27% confidence ellipse, as shown on Figure 4. Among the 22 unique antennas concerned by this issue, 10 are outside the confidence ellipse in both polarizations.

Referring back to the simulations of Figure 2, with the disparity of the 69 antenna patterns of SMOS, the bias and the standard deviation of the reconstruction error map are about 0.7 K and 1.8 K. Shown on Figure 7 is the reconstruction error map obtained with the same modeling of SMOS but with those 10 antenna patterns identified outside the $1\,\sigma$ / 68.27% confidence ellipses modified appropriately with $\alpha = 2$. With this virtual modeling the two components of the floor error are reduced down to 0.5 K and 1.3 K. This is a clear illustration of the impact of the disparity, and specially here on the main contributing antennas, onto the reconstruction floor error. Of course, the reduction is not as important as it would be if all the antennas have benefited from this improvement, as illustrated in Figure 3 where the two components of the floor error are equal to 0.3 K and 0.9 K for $\alpha = 2$. However, this virtual

This article has been accepted for publication in a future issue of this journal, but has not been fully edited. Content may change prior to final publication. Citation information: DOI 10.1109/JSTARS.2020.3022726, IEEE Journal of Selected Topics in Applied Earth Observations and Remote Sensing

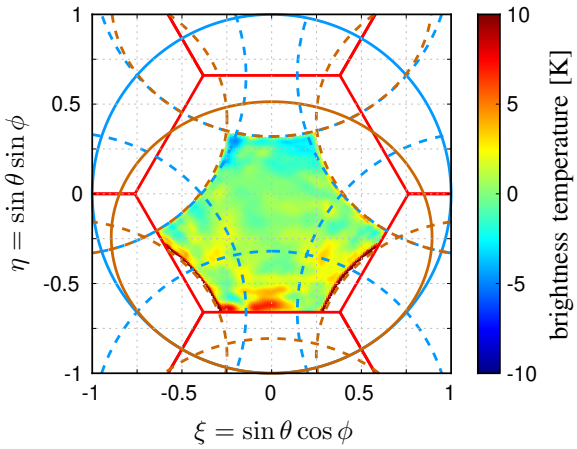

Fig. 7. Error map $\mathcal{T}_r - \mathcal{T}_w$ of simulations performed in X polarization with the current modeling of SMOS equipped with 69 different antenna patterns but with 10 of them identified outside the $1\,\sigma$ / 68.27% confidence ellipses (and only those ones) modified appropriately with $\alpha = 2$. The bias and the standard deviation in that part of the field of view free from Earth aliases are about 0.5 K and 1.3 K. This map has to be compared to the map shown on the left hand of Figure 2 without any modification of these patterns. The same behavior is observed in Y polarization.

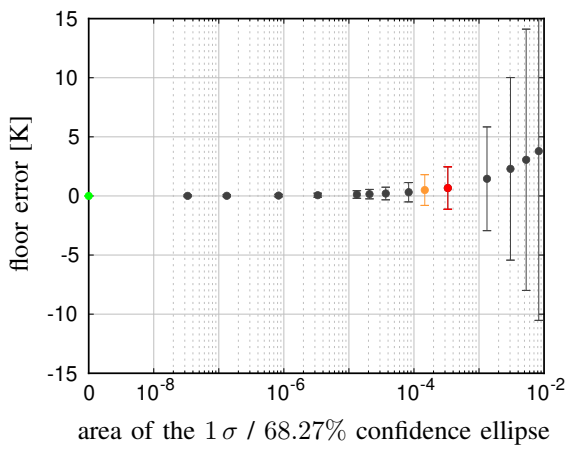

Fig. 8. Same as Figure 3 but here the floor error is reported as a function of the area of the $1\,\sigma$ / 68.27% confidence ellipse in X polarization. In addition to the situation of the current SMOS (red) and to that of an ideal instrument with the same voltage pattern for each antenna (green), the case of an instrument like SMOS (orange) but with 10 antenna patterns identified outside the $1\,\sigma$ / 68.27% confidence ellipses modified appropriately with $\alpha = 2$ is reported for comparison (this case is illustrated in Figure 7). The same behavior is observed in Y polarization.

modification of only 10 out of the 69 patterns made it possible to make half the distance between the present situation of SMOS and a virtual one where the disparity of all 69 patterns would be twice smaller.

As shown on Figure 8 the previous virtual reduction is fully consistent with the decrease of the floor error as the area of the $1\,\sigma$ / 68.27% confidence ellipses decreases. It should be pointed out that here as only 10 patterns have been modified, this virtual case cannot be plotted on Figure 3 where the floor error is reported only when all 69 patterns have been modified. Hence this Figure 8 which does not presuppose the number of modified patterns nor how they were modified, contrary to Figure 3. Finally, a connection between Figures 4 and 8 can be made through the comparison between the distances from the scalar products $\langle F_{ref} \mid F \rangle$ to $\|F_{ref}\|^2 = 1$ and the radii of the disks equivalent to the $1\,\sigma$ / 68.27% confidence ellipses, for example. As a numerical illustration, this radius is equal to 0.0068 for this virtual case shown on Figure 7 and reported in orange on Figure 8. This value can be compared to the distances calculated in Figure 5 for the closest (0.0013) and the farthest (0.0890) antenna patterns.

V. Conclusion

A new metric has been introduced for estimating the disparity between voltage patterns of large data sets of antennas, like those involved in imaging radiometry by aperture synthesis. It is derived from the definition of the equivalent solid angle and inspired from the observing equation of the interferometry in aperture synthesis. Contrary to the well-known equivalent solid angle which is a real-valued quantity of a single antenna, this equivalent cross solid angle is a complex-valued quantity which concerns two antennas. Unlike many other figures of merit, it carries information on the amplitude and on the phase of the two voltage patterns. It can be useful for assessing the accuracy with respect to a given numerical model as well as for evaluating the repeatability associated with the manufacturing of many antennas.

This work is making the connection between the present SMOS mission and the future SMOS*hr* one.

Within the frame of the SMOS mission, the impact of the dissimilarity of the antenna patterns on the reconstruction error observed in the retrieved brightness temperatures has been revisited in light of the progress made since the preliminary design of the instrument. The average voltage pattern has proven to play a particular role in the floor level of the reconstruction error. The usefulness of this new metric has been illustrated with the 69 voltage patterns of SMOS that have been measured prior launch. It has been shown how it is easy to identify those antennas that are the most contributors to the reconstruction floor error because their patterns are too different from the average pattern with respect to this new metric. If this metric had been available at the time these antennas have been built and assembled, it would have been possible to detect them and to conduct specific studies to investigate solutions for reducing the dissimilarity of their patterns and to explore the possibility of manufacturing others with different requirements connected to the target level for the reconstruction floor error in the retrieved brightness temperatures.

Within the frame of the SMOS*hr* project, a research and technology study is currently conducted at industrial level on the design of the future antennas for this new generation of imaging radiometer by aperture synthesis with high resolution performances. Thanks to the lessons learned from SMOS, finite element simulations of the radiation patterns of the 231 antennas are carried on with the aid of the full-wave solver of CST Studio Suite [36], instead of using parametric models that have proven their total inefficiency. As co-design is the new paradigm [37], time consuming end-to-end simulations with engineers, scientists and end-users actively involved are playing an ongoing role for assessing the sensitivity and the

robustness of mission performances to driving parameters, to instrument errors and noises as well as to data processing. This new metric is therefore particularly useful for this purpose, as soon as antenna patterns are all the more concerned in the reduction of the reconstruction floor error as they are many.

REFERENCES

[1] H. Barré, B. Duesmann and Y.H. Kerr, *SMOS: the mission and the system*, IEEE Transactions on Geoscience and Remote Sensing, 46(**3**), pp. 587-593, Mar. 2008.

[2] Y.H. Kerr *et al.*, *The SMOS Soil Moisture Retrieval Algorithm*, 50(**5**), pp. 1384-1403, May 2012.

[3] S. Zine *et al.*, *Overview of the SMOS sea surface salinity prototype processor*, 46(**3**), pp. 621645, Mar. 2008.

[4] P. de Rosnay, N Rodriguez-Fernandez, J Munoz-Sabater, C. Albergel, D. Fairbairn, H. Lawrence, S. English, M. Drusch and Y.H. Kerr , *SMOS Data Assimilation for Numerical Weather Prediction*, Proc. International Geoscience And Remote Sensing Symposium (IGARSS 2018), Valencia (Spain), pp. 1447-1450, Jul. 2018.

[5] N.J. Rodriguez-Fernandez *et al.*, *SMOS-HR: A High Resolution L-Band Passive Radiometer for Earth Science and Applications*, Proc. International Geoscience And Remote Sensing Symposium (IGARSS 2019), Yokohama (Japan), pp. 8392-8395, Jul. 2019.

[6] F. Zheng and M. Chen, *New Conceptual Structure Design for Affordable Space Large Deployable Antenna*, IEEE Transactions on Antennas and Propagation, 63(**4**), pp. 1351-1358, Apr. 2015.

[7] K.D. McMullan, M.A. Brown, M. Martín-Neira, W. Rits, S. Ekholm and J. Lemanczyk, *SMOS: the payload*, IEEE Transactions on Geoscience and Remote Sensing, 46(**3**), pp. 594-605, Mar. 2008.

[8] A.R. Thompson, J.W. Moran and G.W. Swenson, *Interferometry and Synthesis in Radio Astronomy*, Springer, 3rd edition (872 pages), 2017.

[9] É. Anterrieu *et al.*, *Preliminary System Studies on a High-Resolution SMOS Follow-On: SMOS-HR*, Proc. International Geoscience And Remote Sensing Symposium (IGARSS 2019), Yokohama (Japan), pp. 8451-8454, Jul. 2019.

[10] L. Wu *et al.*, *Practical issues on SMOS single antenna patterns*, Proc. 13th Specialist Meeting on Microwave Radiometry and Remote Sensing of the Environment (MicroRad 2014), Pasadena (CA), pp. 197-200, Mar. 2014.

[11] R. Díez-García and M. Martín-Neira, *Analysis and characterization of the reconstruction error in interferometric synthetic aperture imaging radiometers*, Proc. 13th Specialist Meeting on Microwave Radiometry and Remote Sensing of the Environment (MicroRad 2014), Pasadena (CA), pp. 141-146, Mar. 2014.

[12] S. Pivnenko, J.M. Nielsen, C. Cappellin, G. Lemanczyk and O. Breinbjerg, *High-Accuracy Calibration of the SMOS Radiometer Antenna Patterns at the DTU-ESA Spherical Near-Field Antenna Test Facility*, Proc. International Geoscience And Remote Sensing Symposium (IGARSS 2007), Barcelona (Spain), pp. 1-7, Jul. 2007

[13] I. Corbella, N. Duffo, M. Vall-llossera, A. Camps, and F. Torres, *The Visibility Function in Interferometric Aperture Synthesis Radiometry*, IEEE Transactions on Geoscience and Remote Sensing, 42(**8**), pp. 1677-1682, Aug. 2004.

[14] É. Anterrieu and A. Khazâal, *Brightness temperature maps reconstruction from dual-polarimetric visibilities in synthetic aperture imaging radiometry*, IEEE Transactions on Geoscience and Remote Sensing, 46(**3**), pp. 606-612, Mar. 2008.

[15] M. Martín-Neira, S. Ribó and A.J. Martín-Polegre, *Polarimetric mode of MIRAS*, IEEE Transactions on Geoscience and Remote Sensing, 40(**8**), pp. 1755-1768, Aug. 2002.

[16] M. Martín-Neira, M. Suess, and J. Kainulainen, *The Flat Target Transformation*, IEEE Transactions on Geoscience and Remote Sensing, 46(**3**), pp. 613620, Mar. 2008.

[17] I. Corbella, F. Torres, A. Camps, N. Duffo and M. Vall-llossera, *Brightness-Temperature Retrieval Methods in Synthetic Aperture Radiometers*, IEEE Transactions on Geoscience and Remote Sensing, 47(**1**), pp. 285294, Jan. 2009.

[18] M.A. Goodberlet, *Improved image reconstruction techniques for synthetic aperture radiometers*, IEEE Transactions on Geoscience and Remote Sensing, 38(**3**), pp. 1362-1366, May 2000.

[19] É. Anterrieu, P. Waldteufel and A. Lannes, *Apodization functions for 2D hexagonally sampled synthetic aperture imaging radiometers*, IEEE Transactions on Geoscience and Remote Sensing, 40(**12**), pp. 2531-2542, Dec. 2002.

[20] É. Anterrieu, *On the reduction of the reconstruction bias in synthetic aperture imaging radiometry*, IEEE Transactions on Geoscience and Remote Sensing, 45(**3**), pp. 592-601, Mar. 2007.

[21] R. Díez-García and M. Martín-Neira, *Antenna spacing and pattern differences: their impact in MIRAS reconstruction error*, Proc. 14th Specialist Meeting on Microwave Radiometry and Remote Sensing of the Environment (MicroRad 2016), Espoo (Finland), pp. 19-24, Apr. 2016.

[22] É. Anterrieu, M. Suess, F. Cabot, P. Spurgeon and A. Khazâal, *An additive mask correction approach for reducing the systematic floor error in imaging radiometry by aperture synthesis*, IEEE Geoscience and Remote Sensing Letters, 12(**7**), pp. 1441-1445, Jul. 2015.

[23] A. Khazâal, H. Carfantan and É. Anterrieu, *On the reduction of the systematic error in imaging radiometry by aperture synthesis: a new approach for the SMOS space mission*, IEEE Geoscience and Remote Sensing Letters, 6(**1**), pp. 47-51, Jan. 2009.

[24] M. Martín-Neira *et al.*, *SMOS Instrument Performance after More than 9 Years in Orbit*, Proc. International Geoscience And Remote Sensing Symposium (IGARSS 2019), Yokohama (Japan), pp. 8944-8947, Jul. 2019.

[25] I. Corbella, A. Camps, M. Zapata, F. Marcos, F. Martínez, F. Torres, M. Vall-llossera, N. Duffo and J. Bará, *End-to-end simulator of two-dimensional interferometric radiometry*, Radio Science, 38(**3**), pp. 23.1-23.8, Jun. 2003.

[26] B. Picard and É. Anterrieu, *Comparizon of regularized inversion methods in synthetic aperture imaging radiometry*, IEEE Transactions on Geoscience and Remote Sensing, 43(**2**), pp. 218-224, Feb. 2005.

[27] J. McCormick, S.F. Gregson and C.G. Parini, *Quantitative measures of comparison between antenna pattern data sets*, IEE Proceedings - Microwaves, Antennas and Propagation, 152(**6**), pp. 539-550, Dec. 2005.

[28] A.C. Newell and G.E. Hindman, *Antenna pattern comparison using pattern subtraction and statistical analysis*, Proc. European Conference on Antennas and Propagation (EUCAP 2011), Roma (Italy), pp. 2537-2540, Jul. 2011.

[29] É. Anterrieu, S. Gratton and B. Picard, *Self characterization of modelling parameters for synthetic aperture imaging radiometers*, Proc. International Geoscience And Remote Sensing Symposium (IGARSS 2003), Toulouse (France), pp. 3052-3054, Jul. 2003.

[30] C.A. Balanis, *Antenna Theory: Analysis and Design*, Wiley, 3rd edition (1136 pages), 2005.

[31] T.J. Rivlin, *The Chebyshev Polynomials: from Approximation Theory to Algebra and Number Theory*, Wiley, 1st edition (192 pages), 1974.

[32] S. Blanch, J. Romeu and I. Corbella, *Exact representation of antenna system diversity performance from input parameter description*, IET Electronics Letters, 39(**9**), pp. 705-707, May 2003.

[33] A. Camps, N. Skou, F. Torres, I. Corbella,N. Duffo, and M. Vall-llossera, *Considerations About Antenna Pattern Measurements of 2-D Aperture Synthesis Radiometers*, IEEE Geoscience and Remote Sensing Letters, 3(**2**), pp. 259-261, Apr. 2006.

[34] C.D. Ghilani and P.R. Wolf, *Adjustment Computations: Spatial Data Analysis*, Wiley, 4th edition (640 pages), 2006.

[35] M.A. Brown, F. Torres, I. Corbella and A. Colliander, *SMOS calibration*, IEEE Transactions on Geoscience and Remote Sensing, 46(**3**), pp. 646-658, Mar. 2008.

[36] Dassault Systèmes, Computer Simulation Technology, *CST Studio Suite Electromagnetic field simulation software*, www.3ds.com/products-services/simulia/products/cst-studio-suite/

[37] S. Jansen and M. Pieters, *The 7 Principles of Complete Co-Creation*, BIS Publishers, 1st Edition (208 pp), 2018.

Eric Anterrieu (M'02) was born in Brive, France, in 1965. He received the Engineer and the M.S. degrees in solid-state physics from the Institut National des Sciences Appliquées (INSA), Toulouse, France, in 1988, and the M.S. and the Ph.D. degrees in image reconstruction in astronomy from University Paul Sabatier, Toulouse, France, in 1989 and 1992, respectively. The subject of his thesis was the image reconstruction algorithms for multiple aperture interferometry. Since 1993, he has been working as an engineer of research in computer science at the Centre National de la Recherche Scientifique (CNRS). He has been with the Radio and Optical Aperture Synthesis group of LATT (UMR 5572, from 1993 to 2000), with the Signal and Image Processing team of CERFACS (URA 1875, 2000-2004) and with the Signal, Image and Instrumentation group of IRAP (UMR 5277, 2005-2016). Since 2017 he joined CESBIO (UMR 5126) in the Observing Systems team. His present research interests now include numerical analysis, image and signal processing with particular emphasis on the SMOS mission and on the future microwave missions using aperture synthesis and interferometry.

Baptiste Palacin received the Engineer and the M.S. degrees from École Nationale Supérieure d'Électrotechnique, Électronique, Informatique, Hydraulique et Télécommunications (ENSEEIHT), Toulouse, France, in 2008. Since 2009, he has been an antenna engineer in the Antenna department at Centre National d'Études Spatiales (CNES), the French space agency. For several years, he has been working on French telecommunications satellites programs in order to develop the next generation of space multibeam antennas for HTS and VHTS systems. More recently, he has been involved in many French earth observation satellite projects in order to improve satellite antenna performances and system performances of next generation radar altimeter and radiometer to monitor Earth and climate changes.

Laurent Costes was born near Agen, France, in 1963. He is graduated from Paul Sabatier University and Ecole Nationale Suprieure de l'Aéronautique et de l'Espace, Toulouse, France in 1987 in Microwave and Electronics. Since 1989 he has been working as antenna engineer at Airbus Defence and Space (ADS). During the first years he was mainly involved in Telecom satellites developments (LOCSTAR, HISPASAT) and in microwave radiometry since 1993. His activities covered microwave instruments studies and flight developments for ESA and CNES as an antenna architect (MIRAS the first SMOS demonstrator, MHS the Microwave Humidity Sounder for MetOp, MADRAS the multichannel radiometer of MEGHA-TROPIQUES). More recently he was the antenna architect for MWS, the microwave sounder of MetOp-SG and he was responsible of the CIMR (Copernicus Imaging Microwave Radiometer) proposal for the antenna part, a multi-frequency reflector antenna with an 8-meter deployable reflector. He is now an antenna expert in ADS being involved in nearly all studies and developments related to passive radiometry mainly, but also military programs or radar projects.